Atmos. Chem. Phys., 17, 10753–10766, 2017
https://doi.org/10.5194/acp-17-10753-2017

Atmospheric Chemistry and Physics
Open Access
EGU

Estimation of the fossil fuel component in atmospheric CO_2 based on radiocarbon measurements at the Beromünster tall tower, Switzerland

Tesfaye A. Berhanu[1], Sönke Szidat[2], Dominik Brunner[3], Ece Satar[1], Rüdiger Schanda[1], Peter Nyfeler[1], Michael Battaglia[2], Martin Steinbacher[3], Samuel Hammer[4], and Markus Leuenberger[1]

[1]Climate and Environmental Physics, Physics Institute and Oeschger Centre for Climate Change Research, University of Bern, Bern, Switzerland
[2]Department of Chemistry and Biochemistry and Oeschger Center for Climate Change Research, University of Bern, Bern, Switzerland
[3]Empa, Laboratory for Air Pollution/Environmental Technology, Dübendorf, Switzerland
[4]Institut für Umweltphysik, Universität Heidelberg, Heidelberg, Germany

Correspondence to: Tesfaye A. Berhanu (berhanu@climate.unibe.ch)

Received: 25 February 2017 – Discussion started: 20 March 2017
Revised: 7 August 2017 – Accepted: 17 August 2017 – Published: 13 September 2017

Abstract. Fossil fuel CO_2 (CO_{2ff}) is the major contributor of anthropogenic CO_2 in the atmosphere, and accurate quantification is essential to better understand the carbon cycle. Since October 2012, we have been continuously measuring the mixing ratios of CO, CO_2, CH_4, and H_2O at five different heights at the Beromünster tall tower, Switzerland. Air samples for radiocarbon ($\Delta^{14}CO_2$) analysis have also been collected from the highest sampling inlet (212.5 m) of the tower on a biweekly basis. A correction was applied for $^{14}CO_2$ emissions from nearby nuclear power plants (NPPs), which have been simulated with the Lagrangian transport model FLEXPART-COSMO. The $^{14}CO_2$ emissions from NPPs offset the depletion in ^{14}C by fossil fuel emissions, resulting in an underestimation of the fossil fuel component in atmospheric CO_2 by about 16 %. An average observed ratio (R_{CO}) of 13.4 ± 1.3 mmol mol^{-1} was calculated from the enhancements in CO mixing ratios relative to the clean-air reference site Jungfraujoch (ΔCO) and the radiocarbon-based fossil fuel CO_2 mole fractions. The wintertime R_{CO} estimate of 12.5 ± 3.3 is about 30 % higher than the wintertime ratio between in situ measured CO and CO_2 enhancements at Beromünster over the Jungfraujoch background (8.7 mmol mol^{-1}) corrected for non-fossil contributions due to strong biospheric contribution despite the strong correlation between ΔCO and ΔCO_2 in winter. By combining the ratio derived using the radiocarbon measurements and the in situ measured CO mixing ratios, a high-resolution time series of CO_{2ff} was calculated exhibiting a clear seasonality driven by seasonal variability in emissions and vertical mixing. By subtracting the fossil fuel component and the large-scale background, we have determined the regional biospheric CO_2 component that is characterized by seasonal variations ranging between −15 and +30 ppm. A pronounced diurnal variation was observed during summer modulated by biospheric exchange and vertical mixing, while no consistent pattern was found during winter.

1 Introduction

Fossil fuel CO_2 (CO_{2ff}) is the fundamental contributor to the increase in atmospheric CO_2; hence its precise quantification is crucial to better understand the global carbon budget. One of the major uncertainties in the projections of climate change is the uncertainty in the future carbon budget due to feedbacks between terrestrial ecosystems and climate (Heimann and Reichstein, 2008). Information on the response of the biosphere to climate variations can be obtained from atmospheric CO_2 observations, but isolating the biospheric signal in the measured CO_2 mixing ratios requires an accurate quantification of the fossil fuel component. Several

methods have therefore been proposed for quantifying CO_{2ff}, which are based on observations or models. A widely employed approach is to determine CO_{2ff} with an atmospheric transport model that incorporates CO_{2ff} emissions from a bottom-up emission inventory.

Emission inventories are based on statistics of the energy use by different sectors and the quantification of CO_{2ff} emissions by accounting for the carbon content of each fuel and its corresponding oxidation ratios (Friedlingstein et al., 2010; Le Quéré et al., 2016). When compared to other greenhouse gases, national emission inventories for CO_2 are quite accurate, but the computation of these inventories is laborious, and the quality depends on the energy statistics and reporting methods that vary greatly between countries (Marland, 2008; Marland et al., 2009). A recent study evaluating different energy statistics and cement production data estimated an uncertainty of about 5 % for the global fossil fuel emissions of the past decade (2006–2015) (Le Quéré et al., 2016). At country level the uncertainties are usually below 5 % in developed countries but often exceed 10 % in developing countries (Ballantyne et al., 2015).

Additional uncertainties arise from the spatial and temporal disaggregation of national annual total emissions to the grid of the atmospheric transport model. At sub-country scales (less than 150 km), the uncertainty from bottom-up estimates can reach up to 50 % (Ciais et al., 2010). Finally, errors in the transport model and the inability to correctly represent point observations in the model may contribute substantially to the uncertainty of model-simulated CO_{2ff} mixing ratios (Tolk et al., 2008; Peylin et al., 2011).

Radiocarbon measurements can be used to directly quantify CO_{2ff} in atmospheric CO_2 observations. Radiocarbon is produced in the upper atmosphere during the reaction of neutrons with nitrogen induced by cosmic rays (Currie, 2004). In addition, nuclear bomb tests in the 1960s led to large radiocarbon input into the atmosphere, which thereafter decreased due to gradual uptake by the oceans and the terrestrial biosphere (Manning et al., 1990; Levin et al., 2010). Nowadays, the decline in atmospheric $^{14}CO_2$ is mainly driven by input from ^{14}C-free fossil fuel CO_2 (Levin et al., 2010). This decline is well detectable at background sites such as Jungfraujoch, Switzerland, and Schauinsland, Germany (Levin et al., 2013). While all reservoirs exchanging carbon with the atmosphere are relatively rich in ^{14}C, fossil fuels (millions of years old) are devoid of ^{14}C due to its radioactive decay with a half-life of 5370 years. Hence, any fossil fuel CO_2 emitted to the atmosphere will dilute the background ^{14}C signal, the so-called Suess effect, which can then be used to unravel recently added fossil fuel CO_2 to the atmosphere (Zondervan and Meijer, 1996; Levin et al., 2003; Gamnitzer et al., 2006; Turnbull et al., 2006, 2009, 2011a, 2014, 2015; Levin and Karstens, 2007; Lopez et al., 2013). However, this depletion can also partially be offset by CO_2 release from the biosphere which has enriched ^{14}C / ^{12}C ratios due to nuclear bomb tests in the 1960s. ^{14}C produced by these tests was absorbed by the land biosphere and is now gradually being released back to the atmosphere (Naegler and Levin, 2009). Another contribution could be direct ^{14}C emissions from nuclear industries (Levin et al., 2010). This technique also enables separation between biospheric and fossil fuel CO_2 components in atmospheric CO_2 observations, and it thus better constrains the biospheric CO_2 fluxes when coupled with inversion models (Basu et al., 2016). The uncertainty in CO_{2ff} estimated by the radiocarbon method is mainly determined by the precision in the ^{14}C measurement, the choice of background, and the uncertainty in the contribution from other sources of ^{14}C such as nuclear power plants (NPPs) (Turnbull et al., 2009).

Despite its importance as a fossil fuel tracer, measurements of ^{14}C are still sparse. The measurements are expensive and laborious, which so far has prevented frequent sampling and has motivated researchers to combine ^{14}C measurements with additional tracers such as CO to enhance spatial and temporal coverage (Gamnitzer et al., 2006; Turnbull et al., 2006, 2011a, 2014, 2015; Levin and Karstens, 2007; Vogel et al., 2010; Lopez et al., 2013). The CO method relies on using high frequency CO measurements and regular calibration of the temporally changing $\Delta CO : \Delta CO_{2ff}$ ratios based on weekly or biweekly ^{14}C measurements. Despite its advantage of providing a proxy for continuous CO_{2ff} data, the method introduces additional uncertainties due to diurnal and seasonal variability in the CO sink, and the presence of multiple non-fossil CO sources such as oxidation of hydrocarbons or wood and biofuel combustion (Gamnitzer et al., 2006). Spatial variations in the $\Delta CO : \Delta CO_2$ ratio across Europe due to different source compositions and environmental regulations, which affect the measured ratios due to changes in air mass origin (Oney et al., 2017), are the main reason for the temporally changing $\Delta CO : \Delta CO_{2ff}$ ratio for a given measurement site. Additionally, variability in the CO / CO_2 emission ratios of the sources can contribute to its spatial and temporal variability (Vogel et al., 2010; Turnbull et al., 2015).

In Switzerland, CO_2 contributes about 82 % of the total greenhouse gas emissions according to the Swiss national emission inventory for 2013, and fossil fuel combustion from the energy sector contributes more than 80 % of the total CO_2 emission (FOEN, 2015b). In order to validate such bottom-up estimates, independent techniques based on atmospheric measurements are desirable. In addition, as mentioned above, the biospheric CO_2 signals can only be estimated with a good knowledge of CO_{2ff}. In this study, we present and discuss $^{14}CO_2$ measurements conducted biweekly between 2013 and 2015 at the Beromünster tall tower in Switzerland. From these samples in combination with background CO, CO_2, and $^{14}CO_2$ measurements at the high-altitude remote location Jungfraujoch, Switzerland, $\Delta / \Delta CO_{2ff}$ ratios (R_{CO}) are derived. These ratios are then combined with the in situ measured ΔCO mixing ratios to estimate a high-resolution time series of atmospheric CO_{2ff} mixing ratios and, by difference, of the biospheric CO_2 component. The influence of

^{14}C emissions from nearby NPPs and correction strategies are also discussed.

2 Methods

2.1 Site description and continuous measurement of CO and CO_2

A detailed description of the Beromünster tall tower measurement system as well as a characterization of the site with respect to local meteorological conditions, seasonal and diurnal variations of greenhouse gases, and regional representativeness can be obtained from previous publications (Oney et al., 2015; Berhanu et al., 2016; Satar et al., 2016). In brief, the tower is located near the southern border of the Swiss Plateau, the comparatively flat part of Switzerland between the Alps in the south and the Jura Mountains in the northwest (47°11′23″ N, 8°10′32″ E, 797 m a.s.l.), which is characterized by intense agriculture and rather high population density (Fig. 1). The tower is 217.5 m tall with access to five sampling heights (12.5, 44.6, 71.5, 131.6, 212.5 m) for measuring CO, CO_2, CH_4, and H_2O using cavity ring-down spectroscopy (CRDS) (Picarro Inc., G-2401). By sequentially switching from the highest to the lowest level, mixing ratios of these trace gases were recorded continuously for 3 min per height, but only the last 60 s was retained for data analysis. The calibration procedure for ambient air includes measurements of reference gases with high and low mixing ratios traceable to international standards (WMO-X2007 for CO_2 and WMO-X2004 for CO and CH_4), as well as target gas and more frequent working gas determinations to ensure the quality of the measurement system. From 2 years of data a long-term reproducibility of 2.79 ppb, 0.05 ppm, and 0.29 ppb for CO, CO_2, and CH_4, respectively, was determined for this system (Berhanu et al., 2016).

2.2 Sampling and CO_2 extraction for isotope analysis

Air samples for $^{14}CO_2$ analysis were collected from the highest inlet usually between 09:00 to 13:00 UTC. At the beginning we collected one sample per month, which was eventually changed to sampling every second week from November 2013 onwards. During each sampling event, three samples were collected over a 15 min interval in 100 L PE-AL-PE bags (TESSERAUX, Germany) from the flush pump exhaust line of the 212.5 m sampling inlet, which has a flow rate of about 9 L min^{-1} at ambient conditions. The sampling interval was chosen to ensure radiocarbon sample collection in parallel with the continuous CO and CO_2 measurements by the CRDS analyzer at the highest level. Each bag was filled at ambient air pressure for 6 to 8 min, and a total air volume of 50 to 70 L (at STP) was collected.

CO_2 extraction was conducted cryogenically in the laboratory at the University of Bern usually the day after the sample collection. During the extraction step, the air sample was first pumped through a stainless-steel water trap (−75 °C), which was filled with glass beads (Raschig rings, 5 mm, Germany). A flow controller (Analyt-MTC, Aalborg, USA) with a flow totalizer tool was attached to this trap to maintain a constant flow of air (1.2 L min^{-1}) towards the second trap (trap 2), a spiral-shaped stainless-steel tube (1/4 in.) filled with glass beads (∼ 2 mm) and immersed in liquid nitrogen to freeze out CO_2. When the flow ceased, trap 2 was isolated from the line and evacuated to remove gases which are non-condensable at this temperature. Then, trap 2 was warmed to room temperature and eventually immersed in slush at −75 °C to freeze out any remaining water. Finally, the extracted CO_2 was expanded and collected in a 50 mL glass flask immersed in liquid nitrogen.

Sample extraction efficiency was calculated by comparing the amount of the cryogenically extracted CO_2 with the CO_2 measured in situ by the CRDS analyzer during the time of sampling. The amount of CO_2 extracted is determined first by transferring the extracted CO_2 cryogenically to a vacuum line of predetermined volume. Then, based on the pressure reading of the expanded gas, and the total volume of air collected determined by the mass flow controller with a totalizer function attached to trap 1, CO_2 mixing ratios were calculated.

At the end of 2014 we noticed that there was a leakage from the sampling line exhaust pumps, which resulted in unrealistically high CO_2 mixing ratios (usually more than 500 ppm). Therefore, we replaced all the exhaust pumps. To further ensure that the leakage problem during sampling is solved, we regularly check for leaks before sampling by closing the needle valves leading to the pumps and monitoring in case there is any flow with the flow meter attached after the pump. Since the replacement we have not observed any indication of leakage. Seven samples which were suspected to be contaminated due to this issue were consequently excluded. The sample extraction efficiency since then has usually been better than 99 %. We also conducted a blank test to check the presence of any leaks or contamination during sample processing but did not observe any of these issues. Five more samples were excluded in 2014 due to a strong mismatch among triplicates in the measured CO_2 after the sample extraction which indicated contamination.

2.3 Measurement of $\delta^{13}C$, $\delta^{18}O$, and $\Delta^{14}C$

Prior to radiocarbon measurement, the extracted CO_2 was analyzed for the stable isotopes $\delta^{13}C$ and $\delta^{18}O$ using an isotope ratio mass spectrometer (IRMS, Finnigan MAT 250) at the Climate and Environmental Physics Division of the University of Bern, which has an accuracy and precision of better than 0.1 ‰ for both $\delta^{13}C$ and $\delta^{18}O$ (Leuenberger et al., 2003). ^{14}C analysis of the extracted CO_2 was performed with an accelerator mass spectrometer (AMS), MICADAS (MIni CArbon DAting System), at the Laboratory for the Analysis of Radiocarbon (LARA) at the Department of Chemistry

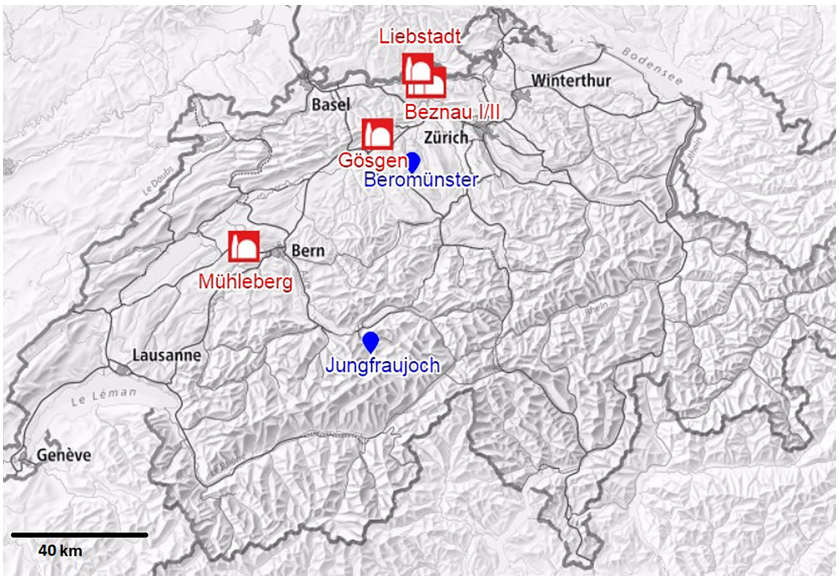

Figure 1. The geographical map of Beromünster and Jungfraujoch measurement sites (blue) as well as the five NPPs in Switzerland (red).

and Biochemistry of the University of Bern (Szidat et al., 2014). The Automated Graphitization Equipment (AGE) was used to prepare solid target gas (Nemec et al., 2010) from the extracted CO_2 stored in 50 mL glass flasks. A measurement series consisted of up to 15 air samples converted to 30 solid graphite targets (duplicates), together with four and three targets from CO_2 produced by combustion of the NIST standard oxalic acid II (SRM 4990C) and fossil CO_2 (Carbagas, Gümligen), respectively, which were used for the blank subtraction, standard normalization, and correction for isotopic fractionations. For the fractionation correction, $\delta^{13}C$ values of the AMS were used, which show a long-term standard uncertainty of ± 1.2 ‰ (Szidat et al., 2014). The AMS $\delta^{13}C$ values agree well on average with the corresponding IRMS results, revealing a statistically insignificant difference of -0.2 ± 1.2 ‰ with slightly more depleted AMS results.

Data reduction was performed using the BATS program (Wacker et al., 2010). The uncertainty of an individual ^{14}C measurement typically amounts to ~ 2.1 ‰, including contributions from counting statistics (~ 1.1 ‰), corrections of normalization (i.e., blank subtraction, standard normalization, and correction for isotopic fractionations) (~ 1.1 ‰), and an unaccounted-for long-term variability of sampling and ^{14}C analysis according to Szidat et al. (2014) (1.5 ‰). These contributions are comparable to previous observations (Graven et al., 2007).

During calculation of weighted averages of the duplicates, the uncertainty of the mean is determined with the contributions of the counting statistics and the normalization, whereas the uncertainty of the unaccounted-for long-term variability is considered fully afterwards, as this contribution cannot be reduced by averaging of two measurements performed on the same day. This uncertainty of the weighted average typically amounts to ~ 1.9 ‰; it is compared with the standard deviation of the duplicates, and the larger of these values is used as the final uncertainty of the duplicates. The mean of the three individual samples from the same day, which is used below in Sect. 2.4.1 as $\Delta^{14}C_{meas}$, is then determined and associated with the average uncertainty of the three duplicates, as the variability of the three samples is comparable to this average uncertainty for all cases.

As the ^{14}C / ^{12}C from Beromünster was measured at the LARA laboratory in Bern, whereas the corresponding background samples from Jungfraujoch were analyzed at the low-level counting (LLC) facility of the Institute of Environmental Physics, Heidelberg University, the data sets needed to be adjusted to each other. A recent interlaboratory compatibility test between the LARA lab (code no. 2) and Heidelberg (LLC) estimated a small bias (Hammer et al., 2016). The measurement bias (i.e., the mean difference of the measured $\Delta^{14}C$ minus the consensus value of the participating laboratories for all investigated CO_2 samples) is $+1.8 \pm 0.1$ and -0.3 ± 0.5 ‰ for Bern and Heidelberg, respectively, from which the bias between both labs of 2.1 ± 0.5 ‰ is determined with a larger measured $\Delta^{14}C$ for Bern. Consequently, 2.1 ± 0.5 ‰ was subtracted from the ^{14}C measurements of the Beromünster samples.

2.4 Determination of the fossil fuel CO_2 component

2.4.1 The $\Delta^{14}C$ technique

For the determination of the CO_{2ff} component we followed approaches similar to those in in previous studies (Zondervan and Meijer, 1996; Levin et al., 2003; Levin and Karstens, 2007; Turnbull et al., 2009). The measured CO_2 is assumed

to be composed of three major components: the free troposphere background (CO_{2bg}), the regional biospheric component (CO_{2bio}) comprising photosynthesis and respiration components, and the fossil fuel component (CO_{2ff}):

$$CO_{2meas} = CO_{2bg} + CO_{2bio} + CO_{2ff} \quad (1)$$

Each of these components has a specific $\Delta^{14}C$ value (i.e., the deviation in per mill of the ^{14}C / ^{12}C ratio from its primary standard, and corrected for fractionation and decay using ^{13}C measurements) described as $\Delta^{14}C_{meas}$, $\Delta^{14}C_{bg}$, $\Delta^{14}C_{bio}$, and $\Delta^{14}C_{ff}$. In analogy to Eq. (1), a mass balance approximation equation can also be formulated for ^{14}C as

$$\begin{aligned} CO_{2meas}\left(\Delta^{14}C_{meas} + 1000‰\right) &= CO_{2bg}\left(\Delta^{14}C_{bg}\right. \\ &\left. + 1000‰\right) + CO_{2bio}\left(\Delta^{14}C_{bio} + 1000‰\right) \\ &+ CO_{2ff}\left(\Delta^{14}C_{ff} + 1000‰\right). \end{aligned} \quad (2)$$

Note that non-fossil-fuel components such as biofuels are incorporated into the biospheric component in Eq. (1). The fossil fuel term in Eq. (2) is zero as fossil fuels are devoid of radiocarbon ($\Delta^{14}C_{ff} = -1000‰$). By replacing the biospheric CO_2 component in Eq. (1) by a formulation derived from Eq. (2), the fossil fuel CO_2 component is derived as

$$CO_{2ff} = \frac{CO_{2bg}\left(\Delta^{14}C_{bg} - \Delta^{14}C_{bio}\right) - CO_{2meas}\left(\Delta^{14}C_{meas} - \Delta^{14}C_{bio}\right)}{\Delta^{14}C_{bio} + 1000‰}. \quad (3)$$

Equation (3) can be further simplified by assuming that $\Delta^{14}C_{bio}$ is equal to $\Delta^{14}C_{bg}$ (Levin et al., 2003) as

$$CO_{2ff} = \frac{CO_{2meas}\left(\Delta^{14}C_{bg} - \Delta^{14}C_{meas}\right)}{\Delta^{14}C_{bg} + 1000‰}. \quad (4)$$

Hence, the fossil fuel CO_2 component can be determined using the CO_{2meas} and $\Delta^{14}C_{meas}$ values measured at the site as well as $\Delta^{14}C_{bg}$ obtained from the Jungfraujoch mountain background site in the Swiss Alps.

However, the CO_{2ff} determined using Eq. (4) incorporates a small bias due to the non-negligible disequilibrium contribution of heterotrophic respiration as well as due to contributions from NPPs. To correct for the bias from these other contributions, an additional term (CO_{2other} and $\Delta^{14}C_{other}$) can be included in Eq. (4) as suggested by Turnbull et al. (2009):

$$\begin{aligned} CO_{2ff} = &\frac{CO_{2meas}\left(\Delta^{14}C_{bg} - \Delta^{14}C_{meas}\right)}{\Delta^{14}C_{bg} + 1000‰} \\ &+ \frac{CO_{2other}\left(\Delta^{14}C_{other} - \Delta^{14}C_{bg}\right)}{\Delta^{14}C_{bg} + 1000‰}, \end{aligned} \quad (5)$$

where CO_{2other} and $\Delta^{14}C_{other}$ represent the additional CO_2 and radiocarbon contributions from other sources such as NPPS and biospheric fluxes, respectively.

The contributions from heterotrophic respiration will lead to an underestimation of CO_{2ff} on average by 0.2 ppm in winter and 0.5 ppm in summer, estimated for the Northern Hemisphere using a mean terrestrial carbon residence time of 10 years (Turnbull et al., 2006).

To account for the bias from heterotrophic respiration, a harmonic function varying seasonally between these values was added to the derived CO_{2ff} values. However, variation of respiration fluxes on shorter timescales cannot be accounted for by this simple correction. The correction strategy for the contribution from NPPs is described in Sect. 2.4.2 below.

2.4.2 Simulation of $^{14}CO_2$ from nuclear power plants

Radiocarbon is produced by nuclear reactions in NPPs and primarily emitted in the form of $^{14}CO_2$ (Yim and Caron, 2006), except for pressurized water reactors (PWRs), which release ^{14}C mainly in the form of $^{14}CH_4$. Previous studies have shown that such emissions can lead to large-scale gradients in atmospheric $\Delta^{14}C$ activity and offset the depletion from fossil fuel emissions (Graven and Gruber, 2011). In Heidelberg, Germany, an offset of 25 and 10 % of the fossil fuel signal was observed during summer and winter, respectively, due to emissions from a nearby plant (Levin et al., 2003). Similarly, Vogel et al. (2013) determined the influence of NPPs for a measurement site in Canada and estimated that about 56 % of the total CO_{2ff} component was masked by the contribution from NPPs, though this large number was obtained for a site in close vicinity of the CANadian Deutrium Uranium-type reactor (CANDU), known for producing particularly high ^{14}C emissions. In Switzerland, there are five NPPs, and the closest plant is located about 30 km to the northwest of Beromünster (Fig. 1). Furthermore, air masses arriving at Beromünster are frequently advected from France, which is the largest producer of nuclear power in Europe.

To estimate the influence of Swiss and other European NPPs on $\Delta^{14}C$ at Beromünster, we used FLEXPART-COSMO backward Lagrangian particle dispersion simulations (Henne et al., 2016). FLEXPART-COSMO was driven by hourly operational analyses of the non-hydrostatic numerical weather prediction model COSMO provided by the Swiss weather service MeteoSwiss at approximately $7 \times 7\,km^2$ resolution for a domain covering large parts of western Europe from the southern tip of Spain to the northern tip of Denmark and from the west coast of Ireland to eastern Poland. For each 3 h measurement interval during the 3-year period, a source sensitivity map (footprint) was calculated by tracing the paths of 50 000 particles released from Beromünster at 212 m above ground over 4 days backward in time. The source sensitivities were then multiplied with the $^{14}CO_2$ emissions of all NPPs within the model domain. Thereby, the emission of a given NPP was distributed over the area of the model grid cell containing the NPP. Source sensitivities were calculated for three different vertical layers (0–50, 50–200, 200–500 m). Since the height of ventilation chimneys of the

Swiss NPPs is between 99 and 120 m, only the sensitivity of the middle layer was selected here as it corresponds best to the effective release height.

The release of ^{14}C both in inorganic (CO_2) and organic form (CH_4) is routinely measured at all Swiss NPPs. Annual totals of ^{14}C emissions are published in the annual reports of the Swiss Federal Nuclear Safety Inspectorate ENSI (https://www.ensi.ch/de/dokumente/document-category/strahlenschutzberichte/). The corresponding data have been kindly provided by the Swiss Federal Nuclear Safety Inspectorate ENSI and the Berner Kraftwerke (BKW), operating the NPP Mühleberg at temporal resolutions ranging from annual (Benznau 1 & 2) to monthly (Leibstadt, Gösgen) and biweekly (Mühleberg), and we assumed constant emissions over the corresponding periods. For Beznau 1, the emissions of 2015 were distributed over the first 3 months of the year due to the shutdown of the plant in March 2015. The largest sources of $^{14}CO_2$ in Switzerland are the two boiling water reactors Mühleberg and Leibstadt (Loosli and Oeschger, 1989). Beznau 1 and 2 and Gösgen are PWRs emitting about 1 order of magnitude less $^{14}CO_2$. For NPPs outside Switzerland, the emissions were estimated from energy production data reported to the International Atomic Energy Agency (IAEA) and NPP type-specific emission factors following Graven and Gruber (2011). The difference $\delta\Delta^{14}C_{nucBRM}$ in $\Delta^{14}C$ between the nuclear emission signals at Beromünster ($\Delta^{14}C_{nucBRM}$) and at Jungfraujcoh ($\Delta^{14}C_{nucJFJ}$) was then computed following Eq. (4) in Levin et al. (2010) and assuming that the mole fraction (n^{14}) of ^{14}C due to NPPs at Jungfraujoch is negligible compared to Beromünster. We then obtain

$$\Delta^{14}C_{nuc} = f\frac{n^{14}_{npp}}{n^{CO_2}_{meas}} + 1000, \quad (6)$$

with the dimensionless factor $f = 8.19 \times 10_{14}$ and $n^{14}_{npp}/n^{CO_2}_{meas}$ being the number of ^{14}C atoms due to NPPs simulated with FLEXPART-COSMO relative to the total number of C atoms ($^{12}C + {}^{13}C + {}^{14}C$) (which is equal to the total number of CO_2 molecules) measured at Beromünster.

2.4.3 Calculation of R_{CO}, ΔCO / ΔCO_2, and high-resolution CO_{2ff}

A $\Delta CO / \Delta CO_{2ff}$ ratio (R_{CO}) was calculated as the slope of the geometric mean regression (model II), with ΔCO being the CO enhancement over a background measured at Jungfraujoch, and the CO_{2ff} values as determined above. The CO measurements at Jungfraujoch were conducted using a CRDS analyzer (Picarro Inc., G-2401) with a measurement precision of ± 2.5 ppb for 1 min aggregates (Zellweger et al., 2012).

As CO is usually co-emitted with CO_2 during incomplete combustion of fossil and other fuels, we have also computed a tracer ratio designated as $\Delta CO / \Delta CO_2$ from the enhancements in the in situ measured CO and CO_2 mixing ratios over the Jungfraujoch background (Oney et al., 2017). CO_{2bg} and CO_{bg} values were obtained by applying the robust extraction of baseline signal (REBS) statistical method (Ruckstuhl et al., 2012) to the continuous CO_2 and CO measurements at the high-altitude site Jungfraujoch (Schibig et al., 2016) with a bandwidth of 60 days. Note that, while R_{CO} strictly refers to the ratio of ΔCO to fossil fuel CO_2 emissions, the $\Delta CO / \Delta CO_2$ ratio can be influenced by biospheric contribution as well as CO_2 emissions from non-fossil sources such as biofuels and biomass burning.

In order to construct the high-resolution CO_{2ff} time series, we combined the in situ measured CO enhancements at the Beromünster tower with the radiocarbon-derived ratios R_{CO} and estimated CO^{CO}_{2ff} for the 3-year data set as

$$CO^{CO}_{2ff} = \frac{CO_{obs} - CO_{bg}}{R_{CO}}, \quad (7)$$

where CO_{obs} is the hourly averaged CO measurements at the tower.

3 Results and discussions

3.1 $\Delta^{14}CO_2$ and CO_{2ff}

Figure 2a shows the in situ measured hourly mean CO_2 dry-air mole fractions at Beromünster (black) from the 212.5 m sample inlet matching at hours when air samples were collected for radiocarbon analysis and the corresponding background CO_2 at Jungfraujoch (blue). During the measurement period, we recorded CO_2 mixing ratios between 389 and 417 ppm. Spikes of CO_2 were observed mainly during winter, associated with weak vertical mixing and enhanced anthropogenic emissions, while lower CO_2 mixing ratios were recorded during summer due to strong vertical mixing and photosynthetic uptake.

Isotopic analysis of the air samples yielded $\Delta^{14}C_{meas}$ between -12.3 and $+22.8$ ‰, with no clear seasonal trend, after correction for the model-simulated contribution from NPPs (Fig. 2b). Based on the simulations described in Sect. 2.4.2, we have calculated a mean enhancement in $\Delta^{14}C$ of $+1.6$ ‰ and a maximum of $+8.4$ ‰ due to NPPs. This agrees qualitatively with the coarse-resolution simulations of Graven and Gruber (2011), which suggest a mean enhancement of $+1.4$ to $+2.8$ ‰ over this region (Graven and Gruber, 2011). While about 70 % of this contribution is due to Swiss NPPs, the remaining contribution is of foreign origin. About 75 % of the contribution from the Swiss NPPs is due to Mühleberg, which is located west of Beromünster and hence frequently upstream of the site, due to the prevailing westerly winds (Oney et al., 2015). Note that each data point represents a mean value of the triplicate samples collected consecutively with a standard error of 2 ‰ among triplicates. During this period, the background $\Delta^{14}C$ values measured at Jungfraujoch varied between 15 and 28 ‰. Regional depletions in $\Delta^{14}C$ due to fossil fuel emissions, i.e.,

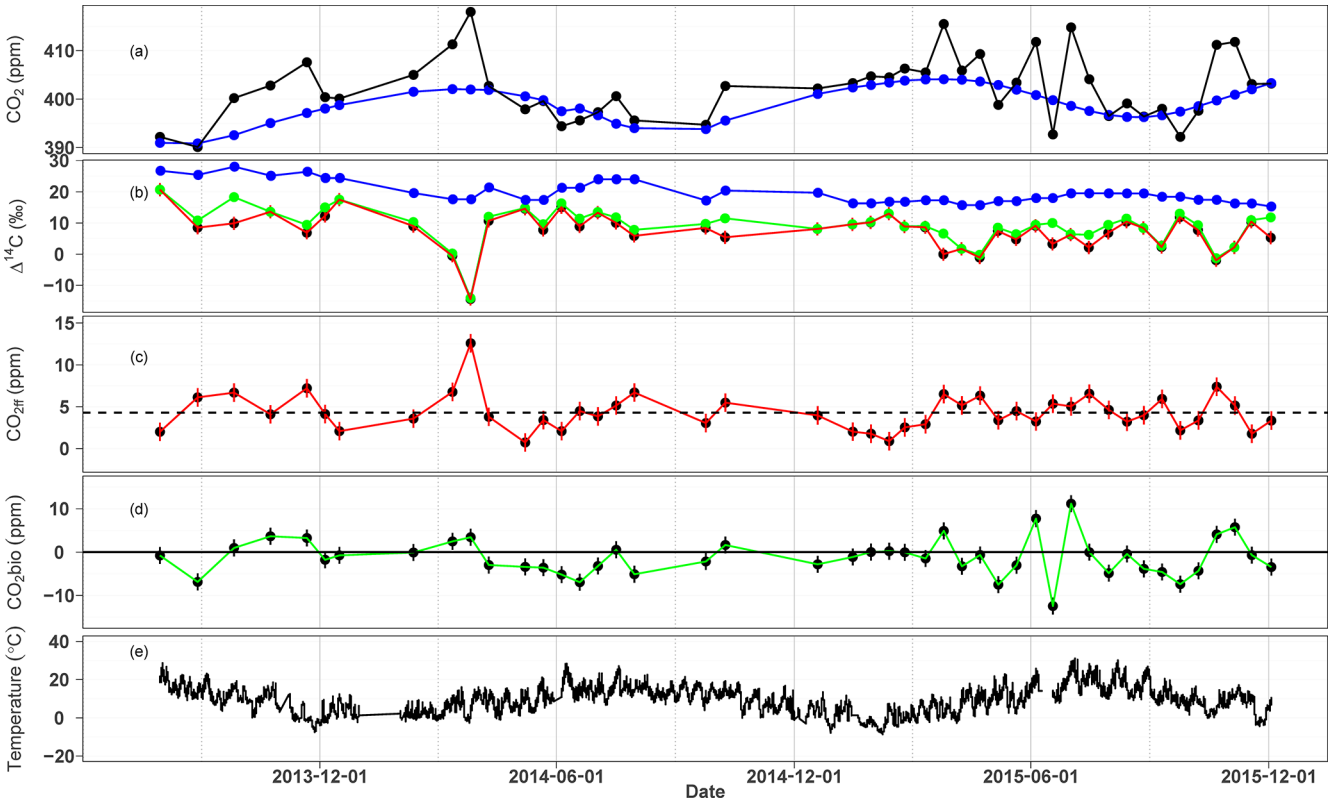

Figure 2. CO_2 mixing ratios (hourly averages) at Beromünster (black) from the sample inlet at 212.5 m and from background measurements at Jungfraujoch (blue) filtered using the REBS function for periods when ^{14}C sampling was conducted **(a)**, $\Delta^{14}C$ determined from the biweekly point samplings at the site before (green) and after (red) correction for the intercomparison offset (see Sect. 2.3) and the ^{14}C contribution from NPPs (see Eq. 5) and from 14-day integrated samplings at Jungfraujoch (blue) **(b)**, CO_{2ff} determined during this period applying Eq. (4) with a mean CO_{2ff} value of 4.3 ppm (dashed line) **(c)**, the biospheric CO_2 determined by simple subtraction of CO_{2bg} and CO_{2ff} from the CO_{2meas} **(d)**, and the temperature record during this period at the 212.5 m height level **(e)**. Error bars in panels **(b)** and **(c)** indicate the mean uncertainty in $\Delta^{14}C$ measurement (±2.0 ‰) and calculated CO_{2ff} (±1.2 ppm), averaged for the triplicate samples, while error bars in panel **(d)** are obtained from error propagation of the components in panels **(a)**, **(b)**, and **(c)**. CO_2 mixing ratios in the top panel are only shown from times matching the radiocarbon sampling at Beromünster tower.

differences between Beromünster and the clean-air reference site Jungfraujoch, were in the range of −0.7 to −29.9 ‰ with a mean value of −9.9 ‰.

Figure 2c shows the corresponding CO_{2ff} determined after correcting for radiocarbon emissions from NPPs. The typical uncertainty in CO_{2ff} is 1.2 ppm calculated by quadratically combining a mean $\Delta^{14}C$ measurement uncertainty of 2.0 ‰ in both the sample and the background values, 0.3 ‰ from biospheric correction, 0.5 ‰ from interlaboratory offset, and a mean uncertainty of 1.2 ‰ in the estimation of ^{14}C contribution from NPPs. A mean fossil fuel CO_2 contribution of 4.3 ppm was calculated from these samples. Few cases, notably the sample from 27 March 2014, showed a higher CO_{2ff} and a strong depletion in $\Delta^{14}C_{meas}$, consistent with the high CO_2 mixing ratio shown in the top panel. This could be due to a strong local fossil fuel contribution or a polluted air mass transported from other regions of Europe coinciding with the grab samplings. As this event occurred during a period with moderate temperatures (mean temperature of 6.8 °C measured at the highest level of the Beromünster tower between March and May), strong fossil fuel CO_2 emissions due to heating are not expected. The FLEXPART-COSMO transport simulations for this event suggest an air mass origin from southeastern Europe (see Supplement). Periods with winds from the east, colloquially known as Bise, are well known to be associated with very stable boundary layers and correspondingly strong accumulation of air pollutants during the cold months of the year between autumn and spring. Air masses reaching Beromünster from eastern Europe have recently been reported to contain unusually high levels of CO during late winter and early spring periods, coinciding with this sampling period (Oney et al., 2017).

By subtracting the background and fossil fuel CO_2 contributions from the measured mixing ratios, CO_{2bio} values were also determined, ranging between +11.2 and −12.4 ppm (Fig. 2d). Even if there is no clear seasonal trend, the lowest CO_{2bio} values were recorded during summer, implying net photosynthetic CO_2 uptake, while most of the values in

Table 1. Ratios (R_{CO}) determined using radiocarbon measurements after correcting for influence from NPPs and applying model II regression, and ratios derived from continuous CO and CO_2 measurements by the CRDS analyzer as enhancements ($\Delta CO : \Delta CO_2$) using Jungfraujoch background measurements. R_{CO} values are given in mmol mol^{-1} with standard uncertainties of the slope and r^2 values in brackets, and n represents the number of samples for the radiocarbon method. Note that, according to the Swiss emission inventory report for greenhouse gas emissions in 2013, the annual anthropogenic CO / CO_2 emission ratio for the national estimate is 7.8 mmol mol^{-1}.

	R_{CO} ($\Delta CO : \Delta CO_{2ff}$) (radiocarbon)	Number of samples (n)	$\Delta CO : \Delta CO_2$ (CRDS)
Winter (Dec–Feb)	12.5 ± 3.3 (0.6)	8	7.3 (0.9)
Summer (Jun–Aug)	14.1 ± 4.0 (0.3)	14	13.4 (0.02)
All data	13.4 ± 1.3 (0.6)	45	8.3 (0.5)

winter are positive or close to zero due to respiration. During summer 2015, we observed strong variability in both CO_2 and CO_{2bio} (Fig. 2a and d). However, this period was one of the hottest and driest summers in central Europe (Orth et al., 2016). In Switzerland, it was the second-hottest summer since the beginning of measurements in 1864 with most of the extreme dates in July (MeteoSuisse, 2015). Such climate extremes can lead to enhanced respiration and reduced photosynthesis and, in turn, higher CO_2 and CO_{2bio} in the atmosphere. Looking specifically at the two data points in June and July 2015, the daily average temperatures recorded at Beromünster were 24.6 and 26 °C at the highest inlet of 212.5 m (Fig. 2e). Based on measurements at Beromünster and other cities of the CarboCount CH network in 2013, Oney et al. (2017) reported that for a daily mean temperature of greater than 20 °C the biosphere over the Swiss plateau tends to become a net CO_2 source. The observed positive spikes in CO_2 (Fig. 2a) and CO_{2bio} (Fig. 2d) likely resulted from such extremes.

3.2 R_{CO} values from radiocarbon measurements

From the simultaneous CO and radiocarbon measurements, we calculated an R_{CO} of 13.4 ± 1.3 mmol CO/mol CO_2 with a correlation coefficient (r^2) of 0.7 and a median value of 11.2 mmol CO/mol CO_2 (note that change in R_{CO} is insignificant when we use smoothed ^{14}C background from Jungfraujoch). When we split the data seasonally, R_{CO} values of 12.5 ± 3.3 and 14.1 ± 4.0 mmol CO/mol CO_2 were obtained during winter and summer, respectively (Table 1). Even if the two values are not significantly different considering the uncertainties, the very low correlation coefficient during summer ($r^2 = 0.3$) implies a larger uncertainty in the derived R_{CO}. Our wintertime estimate is well within the range of values from previous studies (10–15 mmol mol^{-1}) observed at other sites in Europe and North America (Gamnitzer et al., 2006; Vogel et al., 2010; Turnbull et al., 2011a). To test the sensitivity of this ratio to the selection of background site, we additionally calculated R_{CO} using background values estimated with the REBS method from the in situ CO measurements at Beromünster instead of Jungfraujoch. The value obtained in this way (12.7 ± 1.2, $r^2 = 0.6$) is not significantly different from the value obtained using Jungfraujoch as the background site. Considering the persistent decrease in CO emissions (Zellweger et al., 2009) in response to the European emission legislation, our estimated R_{CO} is surprisingly high. A recent study investigating the CO / CO_2 ratio from road traffic in Islisberg tunnel, Switzerland, also observed a significant decrease in this ratio compared to previous estimates, pointing to a substantial reduction in CO emissions from road traffic, with a CO / CO_2 ratio of 4.15 ± 0.34 ppb ppm^{-1} (Popa et al., 2014). This may indicate a significant contribution from non-road traffic emissions, which account for more than 70 % of the total CO_2 emissions leading to the high apparent R_{CO}.

The R_{CO} value derived in this study is significantly higher than the anthropogenic CO / CO_2 emission ratio of 7.8 mmol mol^{-1} calculated from Switzerland's greenhouse gas inventory report for 2013 (FOEN, 2015b, a). However, this can be due to enhanced CO emissions transported from other European cities towards Beromünster. Oney et al. (2017) observed particularly large CO / CO_2 ratios at Beromünster during several pollution events in late winter and early spring 2013 which were associated with air mass transport from eastern Europe, where poorly controlled combustion of biofuels and coal likely results in high ratios.

3.3 ΔCO / ΔCO_2 from continuous measurements

Figure 3 shows the seasonally resolved correlations of ΔCO with ΔCO_2 derived from in situ measured CO and CO_2 enhancements over the background observed at Jungfraujoch, for which we estimated a tracer ratio of 8.3 ± 0.1 mmol mol^{-1} ($r^2 = 0.5$) for the entire measurement period. Considering the seasonally resolved ΔCO / ΔCO_2 ratios, barely any correlation is observed in summer, and weak correlations ($r^2 < 0.4$) are observed during spring and autumn. This can be due to the dominance of biogenic fluxes over fossil fuel fluxes during these periods of the year. From measurements during winter, when the two species are most strongly correlated, a ΔCO / ΔCO_2 ratio of 7.3 ± 0.1 mmol mol^{-1} ($r^2 = 0.9$) is obtained. Recently, Oney et al. (2017) reported a higher wintertime ratio of 8.3 mmol mol^{-1} for the same combination of measurements

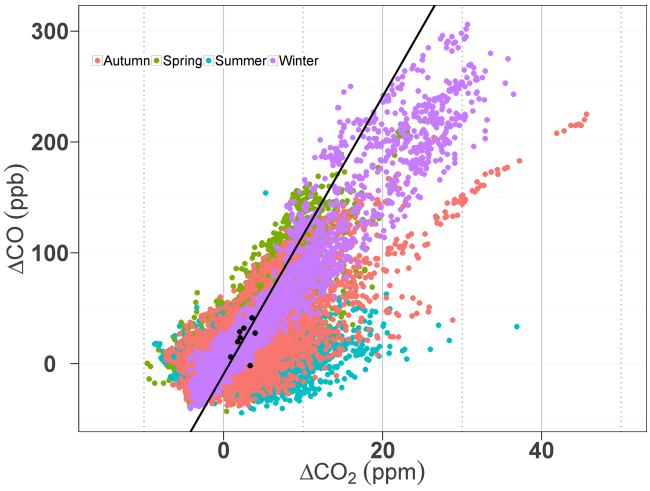

Figure 3. The correlation between enhancements in CO and CO_2 at Beromünster over Jungfraujoch background for the different seasons. The black dots and the black solid line correspond to the individual wintertime R_{CO} values and the linear fit to these points, respectively.

at Beromünster and Jungfraujoch but for a different time period. If we consider only winter 2013 as in their data, we obtain essentially the same value, while much lower ratios of 6.5 and 6.4 mmol mol^{-1} were calculated for 2014 and 2015, respectively. The higher ratios in winter 2013 are likely related to the unusually cold conditions and extended periods of air mass transport from eastern Europe. Note that, in contrast to R_{CO}, these enhancement ratios also include emissions from non-fossil sources such as biofuels and biomass burning as well as the influence of biogenic fluxes. The Swiss national inventory attributes about 15 % of total CO_2 emissions in 2014 to non-fossil-fuel sources (FOEN, 2015b). If we correct for these sources assuming a constant contribution throughout the year, the wintertime ΔCO / ΔCO_2 ratio for the 3-year data becomes 8.7 mmol mol^{-1}.

This ratio of 8.7 mmol mol^{-1} is still about 30 % lower than the R_{CO} estimate for the same period of 12.5 mmol mol^{-1}, shown as a black line in Fig. 3. This suggests that despite the strong correlation between ΔCO and ΔCO_2 in winter the regional CO_2 enhancements are not only caused by anthropogenic emissions but include a significant contribution from biospheric respiration. Miller et al. (2012) showed that such strong correlations between CO_2 and CO during winter may arise from respiratory fluxes co-located with fossil fuel fluxes trapped under the wintertime shallow and stable boundary layer but with strongly biased ratios when compared to R_{CO}. Turnbull et al. (2011b) also observed a substantial contribution of biospheric CO_2 fluxes even during winter (20–30 % from non-fossil-fuel sources including photosynthesis and respiration) from samples collected at two sites in East Asia. The magnitude of these fluxes was roughly similar to the CO_{2ff} flux when continental background was used (Turnbull et al., 2015). Hence, the observed correlation between ΔCO and ΔCO_2 in this study is not only due to spatially and temporally correlated sources but is caused to a large extent by meteorological variability associated with more or less accumulation of trace gases in the boundary layer irrespective of their sources. This interpretation is also supported by the fact that a strong correlation ($r^2 > 0.7$) was also observed between CO and CH_4 during winter at the same tower site (Satar et al., 2016) despite their sources being vastly distinct. In Switzerland about 80 % of CH_4 emissions are from agriculture (mainly from ruminants), while more than 85 % of CO emissions are from the transport sector and residential heating (FOEN, 2015a).

3.4 High-resolution time series of CO_{2ff} and CO_{2bio}

Figure 4 shows the hourly mean CO mixing ratios at Jungfraujoch and Beromünster between 2013 and 2015. CO mixing ratios as high as 480 ppb were recorded at Beromünster, while generally lower CO values were recorded at the more remote site Jungfraujoch. A pronounced seasonality in CO can be observed at Beromünster with higher values in winter and lower values during summer due to stronger vertical mixing and chemical depletion of CO by OH (Satar et al., 2016). The hourly mean CO_{2ff} time series calculated using these continuous CO measurements and the seasonally resolved R_{CO} values derived using the radiocarbon measurements are displayed in Fig. 4c. A seasonal trend in the calculated CO_{2ff} is observed with frequent spikes of CO_{2ff} during winter, while summer values show less variability. We calculated a monthly mean amplitude (peak to trough) of 6.3 ppm with a maximum in February and a minimum in July. During the measurement period, we observed CO_{2ff} mixing ratios ranging up to 27 ppm coinciding with cold periods and likely from enhanced anthropogenic emissions due to heating. Instances of slightly negative CO_{2ff} contributions, which occurred during less than 5 % of the time, were associated with negative enhancements in CO (i.e., $\Delta CO < 0$). This could be simply due to an overestimation of background values by the REBS function during these periods.

Figure 5a shows the hourly averaged residual CO_{2bio} values, which exhibit not only a clear seasonal cycle but also a considerable scatter in all seasons, ranging from −13 to +30 ppm. During winter, most values were close to zero or positive, implying a dominance of respiration fluxes. In summer, conversely, pronounced negative and positive excursions were observed mostly due to the diurnal cycle in net CO_2 fluxes, which are dominated by photosynthetic uptake during daytime and respiration at night. Another factor contributing to such variations may be the application of a constant emission ratio neglecting any diurnal variability (Vogel et al., 2010).

It should also be noted that any non-fossil-fuel CO_2 sources such as emissions from biofuels would be incorporated into the CO_{2bio} term since CO_{2ff} in Eq. (1) represents

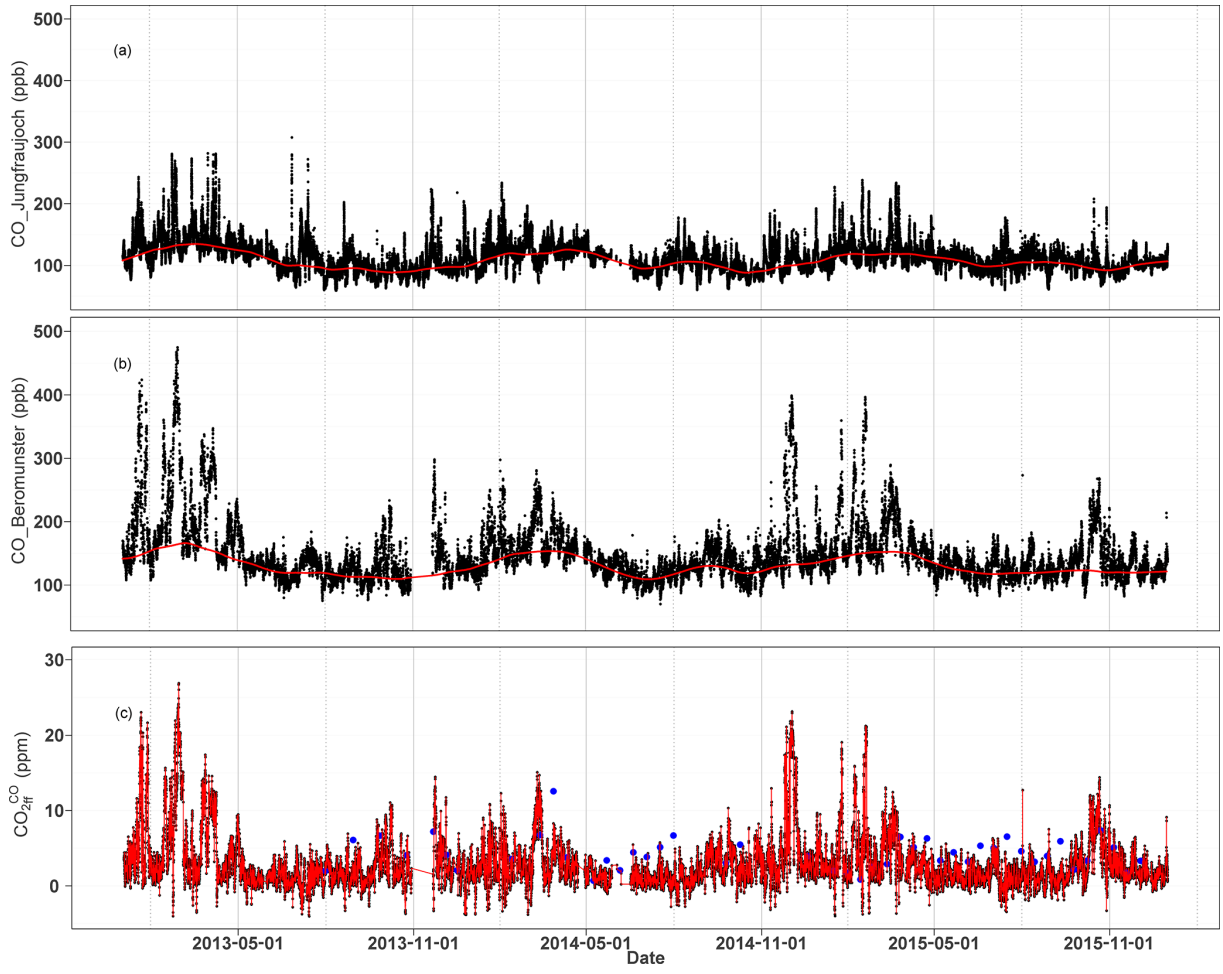

Figure 4. Time series of hourly mean CO mixing ratios measured at Jungfraujoch **(a)** and Beromünster **(b)** sites, with the red curve showing the estimated background values using the REBS method with 60-day window. Panel **(c)** shows the hourly mean CO_{2ff} time series calculated using the emission ratios determined from radiocarbon measurements, and the CO enhancements at Beromünster over the Jungfraujoch background based on Eq. (7). The blue dots in panel **(c)** shows the CO_{2ff} values determined using the radiocarbon measurements.

the fossil fuel sources only, adding more variability to the data set. In order to reduce the influence of these diurnal factors, we have looked into afternoon CO_{2bio} values (12:00–15:00 UTC), when the CO_2 mixing ratios along the tower are uniform (Satar et al., 2016) and R_{CO} variability is minimal. Similar to the seasonal pattern in Fig. 5a, a clear seasonal cycle in biospheric CO_2 can be observed (Fig. 5b) in agreement with biospheric exchange, but both positive and negative extremes are less frequently observed (−12 to +22 ppm).

The variation in CO_{2bio} during afternoon (12:00–15:00 UTC) was recently estimated at this site at a range of −20 to +20 ppm by combining observations and model simulations for the year 2013 (Oney et al., 2017). Our estimates are more positive than those in their study, due to the higher R_{CO} which results in lower CO_{2ff} and correspondingly higher CO_{2bio} values.

Biospheric CO_2 shows a seasonally dependent diurnal variation as shown in Fig. 6. During winter (December–February), the biospheric CO_2 component remains consistently positive (+2 to +5 ppm) throughout the day, implying net respiration fluxes. In summer, a clear feature with increasing CO_{2bio} values during the night peaking between 07:00 and 08:00 UTC (i.e., between 08:00 and 09:00 local time) can be observed. This buildup during the night can be explained by CO_2 from respiration fluxes accumulating in the stable and shallow nocturnal boundary layer. Then, after sunrise, the early morning CO_{2bio} peak starts to gradually decrease due to a combination of onset of photosynthesis and enhanced vertical mixing due to the growth of the boundary layer. At Beromünster, a decrease in CO_2 mixing ratios from both processes is visible more or less at the same time at the 212.5 m height level. As reported by Satar et al. (2016), this decrease in early morning CO_2 concentrations at the 212 m inlet lags behind the decrease at the lowest sampling level of 12.5 m by approximately 1 h. Between 12:00 and 15:00 UTC, when the daytime convective bound-

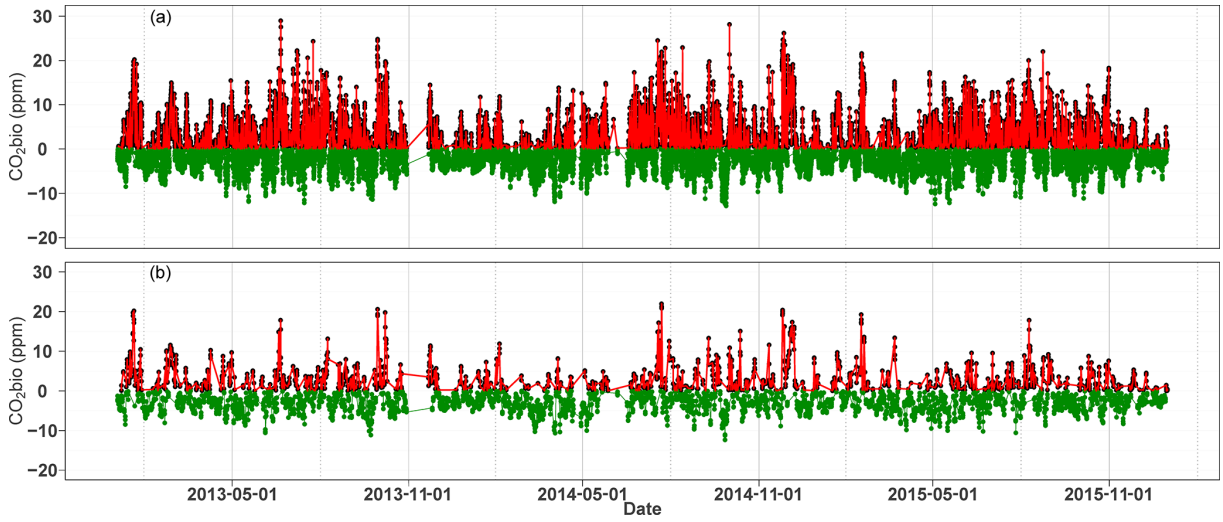

Figure 5. Time series (hourly resolution) of the biospheric CO_2 derived as a residual of the difference between the total CO_2, CO_{2bg}, and CO_{2ff} for all data **(a)**, and only afternoon data from 12:00–15:00 UTC **(b)**. The green lines show negative CO_{2bio}, implying uptake, while red ones represent positive CO_{2bio}. The average uncertainty of CO_{2bio} amounts ±1.3 ppm calculated from error propagation.

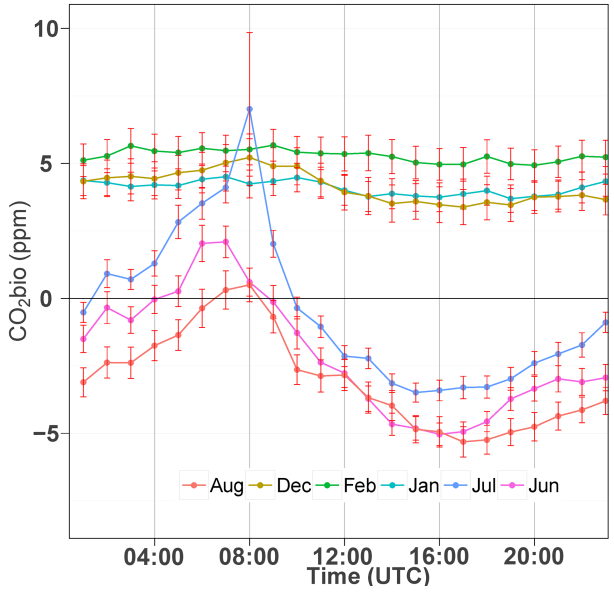

Figure 6. Hourly variations of monthly averaged biospheric CO_2 during summer (June–August) and winter (December–February). While winter values dominated by respiration are constant throughout a day, summer values show a significant diurnal variation induced by photosynthesis and vertical mixing. The error bars are the standard deviations of the hourly averaged CO_{2bio} values for each month.

ary layer is fully established, the biospheric CO_2 continues to become more negative, implying net photosynthetic uptake, which eventually stabilizes for 3–5 h until nighttime CO_{2bio} accumulation starts.

4 Conclusions

From continuous measurements of CO and CO_2 and bi-weekly radiocarbon samples at the Beromünster tall tower, we have estimated a $\Delta CO / \Delta CO_{2ff}$ ratio (R_{CO}) which was subsequently used to construct a 2.3-year-long high-resolution CO_{2ff} time series. We have corrected the ratio for an offset of about 16 % caused by ^{14}C emissions from nearby NPPs. This bias was calculated by comparing the simulated mean enhancement in $\Delta^{14}C$ (1.6 ‰) due to NPPs with the measured mean depletion in $\Delta^{14}C$ due to fossil fuel CO_2 (9.9 ‰). The radiocarbon-based R_{CO} derived in this study during winter is about 30 % higher than the CO:CO_2 enhancement ratios estimated from continuous CO and CO_2 measurements during the same period, suggesting a significant biospheric contribution to regional CO_2 enhancements during this period. This is in agreement with previous studies that observed 20–30 % biospheric contribution during winter (Turnbull et al., 2011b).

The obtained CO_{2ff} time series shows a clear seasonality with frequent spikes during winter associated with enhanced anthropogenic emissions and weak vertical mixing, while summer values are mostly stable.

By subtracting the estimated CO_{2ff} and CO_{2bg} from CO_{2meas}, we have also calculated the biospheric CO_2 component, which ranges between −15 and +30 ppm. Considering only afternoon data (12:00–15:00 UTC), when the convective boundary layer is fully established, CO_{2bio} showed its minimum in summer coinciding with net photosynthetic uptake but still with frequent positive excursions, especially during summer 2015, possibly driven by the record hot and dry summer during this period. During winter, CO_{2bio} becomes nearly zero or positive, implying respiration fluxes.

A pronounced diurnal variation in CO_{2bio} was observed during summer modulated by vertical mixing and biospheric exchange, while this variation disappears during winter. However, the variation in CO_{2bio} may also be influenced by the uncertainty of the CO_{2ff} estimate, especially due to applying a constant emission ratio while calculating CO_{2ff}. Hence, it will be important in the future to include seasonally and diurnally resolved R_{CO} values from high-frequency radiocarbon measurements to better estimate CO_{2ff}. Detailed analysis of the planetary boundary layer height may also provide useful information to better clarify such variations, and it will be the focus of future studies. Additionally, including independent tracers such as atmospheric potential oxygen estimates based on concurrent CO_2 and O_2 measurements will be very useful to validate fossil fuel emission estimates from the radiocarbon method. This technique is also advantageous as the fossil fuel CO_2 estimate is unaltered by contribution from NPPs, and it accounts for the contribution from biofuels.

Data availability. CO_2 measurements are available through the Obspack data set under the Cooperative Global Atmospheric Data Integration Project (2017). Multi-laboratory compilation of atmospheric carbon dioxide data for the period 1957–2016; obspack_co2_1_GLOBALVIEWplus_v3.0_2017-08-11 [Data set]. NOAA Earth System Research Laboratory, Global Monitoring Division. https://doi.org/10.15138/g3cw4q. Carbon monoxide, radioncarbon, CO2ff and CO2bio data can be requested from M. Leuenberger (leuenberger@climate.unibe.ch).

The Supplement related to this article is available online at https://doi.org/10.5194/acp-17-10753-2017-supplement.

Competing interests. The authors declare that they have no conflict of interest.

Acknowledgements. This project was funded by the Swiss National Science Foundation through the Sinergia project CarboCount CH (CRSII2 136273). We are also grateful to ICOS-Switzerland and the International Foundation High Alpine Research Stations Jungfraujoch and Gornergrat. The LARA laboratory would like to thank René Fischer for the production of large CO_2 amounts by combustion of the NIST standard oxalic acid II, and Dejan Husrefovic for the evaluation of the sample transfer line. Finally, we would like to thank Heather Graven and Nicolas Gruber for helpful input regarding radiocarbon emissions from NPPs and the Swiss Federal Nuclear Safety Inspectorate (ENSI) and the Berner Kraftwerke (BKW) for fruitful discussions and providing radiocarbon emission data.

Edited by: Thomas Röckmann
Reviewed by: Jocelyn Turnbull and one anonymous referee

References

Ballantyne, A. P., Andres, R., Houghton, R., Stocker, B. D., Wanninkhof, R., Anderegg, W., Cooper, L. A., DeGrandpre, M., Tans, P. P., Miller, J. B., Alden, C., and White, J. W. C.: Audit of the global carbon budget: estimate errors and their impact on uptake uncertainty, Biogeosciences, 12, 2565–2584, https://doi.org/10.5194/bg-12-2565-2015, 2015.

Basu, S., Miller, J. B., and Lehman, S.: Separation of biospheric and fossil fuel fluxes of CO_2 by atmospheric inversion of CO_2 and $^{14}CO_2$ measurements: Observation System Simulations, Atmos. Chem. Phys., 16, 5665–5683, https://doi.org/10.5194/acp-16-5665-2016, 2016.

Berhanu, T. A., Satar, E., Schanda, R., Nyfeler, P., Moret, H., Brunner, D., Oney, B., and Leuenberger, M.: Measurements of greenhouse gases at Beromünster tall-tower station in Switzerland, Atmos. Meas. Tech., 9, 2603–2614, https://doi.org/10.5194/amt-9-2603-2016, 2016.

Ciais, P., Paris, J. D., Marland, G., Peylin, P., Piao, S. L., Levin, I., Pregger, T., Scholz, Y., Friedrich, R., Rivier, L., Houwelling, S., Schulze, E. D., and Team, C. S.: The European carbon balance. Part 1: fossil fuel emissions, Glob. Change Biol., 16, 1395–1408, https://doi.org/10.1111/j.1365-2486.2009.02098.x, 2010.

Currie, L. A.: The remarkable metrological history of radiocarbon dating [II], J. Res. Natl. Inst. Stan., 109, 185–217, https://doi.org/10.6028/jres.109.013, 2004.

FOEN: Switzerland's Informative Inventory Report 2015, Swiss Federal Office for the Environement, Bern, 2015a.

FOEN: Switzerland's Greenhose Gas Inventory 1990–2013, Swiss Federal Office for the Environment, Bern, 2015b.

Friedlingstein, P., Houghton, R. A., Marland, G., Hackler, J., Boden, T. A., Conway, T. J., Canadell, J. G., Raupach, M. R., Ciais, P., and Le Quere, C.: Update on CO_2 emissions, Nat. Geosci., 3, 811–812, https://doi.org/10.1038/Ngeo1022, 2010.

Gamnitzer, U., Karstens, U., Kromer, B., Neubert, R. E. M., Meijer, H. A. J., Schroeder, H., and Levin, I.: Carbon monoxide: A quantitative tracer for fossil fuel CO_2?, J. Geophys. Res.-Atmos., 111, D22302, https://doi.org/10.1029/2005jd006966, 2006.

Graven, H. D. and Gruber, N.: Continental-scale enrichment of atmospheric $^{14}CO_2$ from the nuclear power industry: potential impact on the estimation of fossil fuel-derived CO_2, Atmos. Chem. Phys., 11, 12339–12349, https://doi.org/10.5194/acp-11-12339-2011, 2011.

Graven, H. D., Guilderson, T. P., and Keeling, R. F.: Methods for high-precision C-14 AMS measurement of atmospheric CO_2 at LLNL, Radiocarbon, 49, 349–356, 2007.

Hammer, S., Friedrich, R., Kromer, B., Cherkinsky, A., Lehman, S. J., Meijer, H. A. J., Nakamura, T., Palonen, V., Reimer, R. W., Smith, A. M., Southon, J. R., Szidat, S., Turnbull, J., and Uchida, M.: Compatibility of Atmospheric $^{14}CO_2$ Measurements: Comparing the Heidelberg Low-Level Counting Facility to International Accelerator Mass Spectrometry (AMS) Laboratories, Radiocarbon, 59, 1–9, https://doi.org/10.1017/RDC.2016.62, 2016.

Heimann, M. and Reichstein, M.: Terrestrial ecosystem carbon dynamics and climate feedbacks, Nature, 451, 289–292, https://doi.org/10.1038/nature06591, 2008.

Henne, S., Brunner, D., Oney, B., Leuenberger, M., Eugster, W., Bamberger, I., Meinhardt, F., Steinbacher, M., and Emmenegger, L.: Validation of the Swiss methane emission inventory by atmospheric observations and inverse modelling, Atmos.

Chem. Phys., 16, 3683–3710, https://doi.org/10.5194/acp-16-3683-2016, 2016.

Le Quéré, C., Andrew, R. M., Canadell, J. G., Sitch, S., Korsbakken, J. I., Peters, G. P., Manning, A. C., Boden, T. A., Tans, P. P., Houghton, R. A., Keeling, R. F., Alin, S., Andrews, O. D., Anthoni, P., Barbero, L., Bopp, L., Chevallier, F., Chini, L. P., Ciais, P., Currie, K., Delire, C., Doney, S. C., Friedlingstein, P., Gkritzalis, T., Harris, I., Hauck, J., Haverd, V., Hoppema, M., Klein Goldewijk, K., Jain, A. K., Kato, E., Körtzinger, A., Landschützer, P., Lefèvre, N., Lenton, A., Lienert, S., Lombardozzi, D., Melton, J. R., Metzl, N., Millero, F., Monteiro, P. M. S., Munro, D. R., Nabel, J. E. M. S., Nakaoka, S.-I., O'Brien, K., Olsen, A., Omar, A. M., Ono, T., Pierrot, D., Poulter, B., Rödenbeck, C., Salisbury, J., Schuster, U., Schwinger, J., Séférian, R., Skjelvan, I., Stocker, B. D., Sutton, A. J., Takahashi, T., Tian, H., Tilbrook, B., van der Laan-Luijkx, I. T., van der Werf, G. R., Viovy, N., Walker, A. P., Wiltshire, A. J., and Zaehle, S.: Global Carbon Budget 2016, Earth Syst. Sci. Data, 8, 605–649, https://doi.org/10.5194/essd-8-605-2016, 2016.

Leuenberger, M. C., Eyer, M., Nyfeler, P., Stauffer, B., and Stocker, T. F.: High-resolution ^{13}C measurements on ancient air extracted from less than 10 cm(3) of ice, Tellus B, 55, 138–144, https://doi.org/10.1034/j.1600-0889.2003.01463.x, 2003.

Levin, I. and Karstens, U.: Inferring high-resolution fossil fuel CO_2 records at continental sites from combined $^{14}CO_2$ and CO observations, Tellus B, 59, 245–250, https://doi.org/10.1111/j.1600-0889.2006.00244.x, 2007.

Levin, I., Kromer, B., Schmidt, M., and Sartorius, H.: A novel approach for independent budgeting of fossil fuel CO_2 over Europe by $^{14}CO_2$ observations, Geophys. Res. Lett., 30, 2194, https://doi.org/10.1029/2003gl018477, 2003.

Levin, I., Naegler, T., Kromer, B., Diehl, M., Francey, R. J., Gomez-Pelaez, A. J., Steele, L. P., Wagenbach, D., Weller, R., and Worthy, D. E.: Erratum: Observations and modelling of the global distribution and long-term trend of atmospheric $^{14}CO_2$ (vol. 62, 26–46, 2010), Tellus B, 62, p. 207, https://doi.org/10.1111/j.1600-0889.2010.00456.x, 2010.

Levin, I., Kromer, B., and Hammer, S.: Atmospheric Delta $^{14}CO_2$ trend in Western European background air from 2000 to 2012, Tellus B, 65, 20092, https://doi.org/10.3402/tellusb.v65i0.20092, 2013.

Loosli, H. H. and Oeschger, H.: C-14 in the Environment of Swiss Nuclear Installations, Radiocarbon, 31, 747–753, 1989.

Lopez, M., Schmidt, M., Delmotte, M., Colomb, A., Gros, V., Janssen, C., Lehman, S. J., Mondelain, D., Perrussel, O., Ramonet, M., Xueref-Remy, I., and Bousquet, P.: CO, NO_x and $^{13}CO_2$ as tracers for fossil fuel CO_2: results from a pilot study in Paris during winter 2010, Atmos. Chem. Phys., 13, 7343–7358, https://doi.org/10.5194/acp-13-7343-2013, 2013.

Manning, M. R., Lowe, D. C., Melhuish, W. H., Sparks, R. J., Wallace, G., Brenninkmeijer, C. A. M., and Mcgill, R. C.: The Use of Radiocarbon Measurements in Atmospheric Studies, Radiocarbon, 32, 37–58, 1990.

Marland, G.: Uncertainties in accounting for CO_2 from fossil fuels, J. Ind. Ecol., 12, 136–139, https://doi.org/10.1111/j.1530-9290.2008.00014.x, 2008.

Marland, G., Hamal, K., and Jonas, M.: How Uncertain Are Estimates of CO_2 Emissions?, J. Ind. Ecol., 13, 4–7, https://doi.org/10.1111/j.1530-9290.2009.00108.x, 2009.

MétéoSuisse: Bulletin climatologique été 2015, Département fédéral de l'intérieur DFI Office fédéral de météorologie et de climatologie MétéoSuisse, Genève, 2015.

Miller, J. B., Lehman, S. J., Montzka, S. A., Sweeney, C., Miller, B. R., Karion, A., Wolak, C., Dlugokencky, E. J., Southon, J., Turnbull, J. C., and Tans, P. P.: Linking emissions of fossil fuel CO_2 and other anthropogenic trace gases using atmospheric $^{14}CO_2$, 117, https://doi.org/10.1029/2011JD017048, 2012.

Naegler, T. and Levin, I.: Observation-based global biospheric excess radiocarbon inventory 1963–2005, J. Geophys. Res.-Atmos., 114, D17303, https://doi.org/10.1029/2008JD011100, 2009.

Nemec, M., Wacker, L., and Gaggeler, H.: Optimization of the Graphitization Process at Age-1, Radiocarbon, 52, 1380–1393, 2010.

Oney, B., Henne, S., Gruber, N., Leuenberger, M., Bamberger, I., Eugster, W., and Brunner, D.: The CarboCount CH sites: characterization of a dense greenhouse gas observation network, Atmos. Chem. Phys., 15, 11147–11164, https://doi.org/10.5194/acp-15-11147-2015, 2015.

Oney, B., Gruber, N., Henne, S., Leuenberger, M., and Brunner, D.: A CO-based method to determine the regional biospheric signal in atmospheric, Tellus B, 69, 1353388, https://doi.org/10.1080/16000889.2017.1353388, 2017.

Orth, R., Zscheischler, J., and Seneviratne, S. I.: Record dry summer in 2015 challenges precipitation projections in Central Europe, Sci. Rep., 6, 28334, https://doi.org/10.1038/srep28334, 2016.

Peylin, P., Houweling, S., Krol, M. C., Karstens, U., Rödenbeck, C., Geels, C., Vermeulen, A., Badawy, B., Aulagnier, C., Pregger, T., Delage, F., Pieterse, G., Ciais, P., and Heimann, M.: Importance of fossil fuel emission uncertainties over Europe for CO_2 modeling: model intercomparison, Atmos. Chem. Phys., 11, 6607–6622, https://doi.org/10.5194/acp-11-6607-2011, 2011.

Popa, M. E., Vollmer, M. K., Jordan, A., Brand, W. A., Pathirana, S. L., Rothe, M., and Röckmann, T.: Vehicle emissions of greenhouse gases and related tracers from a tunnel study: $CO : CO_2$, $N_2O : CO_2$, $CH_4 : CO_2$, $O_2 : CO_2$ ratios, and the stable isotopes ^{13}C and ^{18}O in CO_2 and CO, Atmos. Chem. Phys., 14, 2105–2123, https://doi.org/10.5194/acp-14-2105-2014, 2014.

Ruckstuhl, A. F., Henne, S., Reimann, S., Steinbacher, M., Vollmer, M. K., O'Doherty, S., Buchmann, B., and Hueglin, C.: Robust extraction of baseline signal of atmospheric trace species using local regression, Atmos. Meas. Tech., 5, 2613–2624, https://doi.org/10.5194/amt-5-2613-2012, 2012.

Satar, E., Berhanu, T. A., Brunner, D., Henne, S., and Leuenberger, M.: Continuous $CO_2/CH_4/CO$ measurements (2012–2014) at Beromünster tall tower station in Switzerland, Biogeosciences, 13, 2623–2635, https://doi.org/10.5194/bg-13-2623-2016, 2016.

Schibig, M. F., Mahieu, E., Henne, S., Lejeune, B., and Leuenberger, M. C.: Intercomparison of in situ NDIR and column FTIR measurements of CO_2 at Jungfraujoch, Atmos. Chem. Phys., 16, 9935–9949, https://doi.org/10.5194/acp-16-9935-2016, 2016.

Szidat, S., Salazar, G. A., Vogel, E., Battaglia, M., Wacker, L., Synal, H. A., and Turler, A.: ^{14}C Analysis and Sample Preparation at the New Bern Laboratory for the Analysis of Radiocarbon with AMS (LARA), Radiocarbon, 56, 561–566, https://doi.org/10.2458/56.17457, 2014.

Tolk, L. F., Meesters, A. G. C. A., Dolman, A. J., and Peters, W.: Modelling representation errors of atmospheric CO_2 mixing ra-

tios at a regional scale, Atmos. Chem. Phys., 8, 6587–6596, https://doi.org/10.5194/acp-8-6587-2008, 2008.

Turnbull, J. C., Miller, J. B., Lehman, S. J., Tans, P. P., Sparks, R. J., and Southon, J.: Comparison of $^{14}CO_2$, CO, and SF6 as tracers for recently added fossil fuel CO_2 in the atmosphere and implications for biological CO_2 exchange, Geophys. Res. Lett., 33, L01817 https://doi.org/10.1029/2005gl024213, 2006.

Turnbull, J. C., Rayner, P., Miller, J., Naegler, T., Ciais, P., and Cozic, A.: On the use of $^{14}CO_2$ as a tracer for fossil fuel CO_2: Quantifying uncertainties using an atmospheric transport model, J. Geophys. Res.-Atmos., 114, D22302, https://doi.org/10.1029/2009jd012308, 2009.

Turnbull, J. C., Karion, A., Fischer, M. L., Faloona, I., Guilderson, T., Lehman, S. J., Miller, B. R., Miller, J. B., Montzka, S., Sherwood, T., Saripalli, S., Sweeney, C., and Tans, P. P.: Assessment of fossil fuel carbon dioxide and other anthropogenic trace gas emissions from airborne measurements over Sacramento, California in spring 2009, Atmos. Chem. Phys., 11, 705–721, https://doi.org/10.5194/acp-11-705-2011, 2011a.

Turnbull, J. C., Tans, P. P., Lehman, S. J., Baker, D., Conway, T. J., Chung, Y. S., Gregg, J., Miller, J. B., Southon, J. R., and Zhou, L. X.: Atmospheric observations of carbon monoxide and fossil fuel CO2 emissions from East Asia, J. Geophys. Res.-Atmos., 116, D24306, https://doi.org/10.1029/2011jd016691, 2011b.

Turnbull, J. C., Keller, E. D., Baisden, T., Brailsford, G., Bromley, T., Norris, M., and Zondervan, A.: Atmospheric measurement of point source fossil CO_2 emissions, Atmos. Chem. Phys., 14, 5001–5014, https://doi.org/10.5194/acp-14-5001-2014, 2014.

Turnbull, J. C., Sweeney, C., Karion, A., Newberger, T., Lehman, S. J., Tans, P. P., Davis, K. J., Lauvaux, T., Miles, N. L., Richardson, S. J., Cambaliza, M. O., Shepson, P. B., Gurney, K., Patarasuk, R., and Razlivanov, I.: Toward quantification and source sector identification of fossil fuel CO_2 emissions from an urban area: Results from the INFLUX experiment, J. Geophys. Res.-Atmos., 120, 292–312, https://doi.org/10.1002/2014jd022555, 2015.

Vogel, F. R., Hammer, S., Steinhof, A., Kromer, B., and Levin, I.: Implication of weekly and diurnal ^{14}C calibration on hourly estimates of CO-based fossil fuel CO_2 at a moderately polluted site in southwestern Germany, Tellus B, 62, 512–520, https://doi.org/10.1111/j.1600-0889.2010.00477.x, 2010.

Vogel, F. R., Levin, I., and Worthy, D. E. J.: Implications for Deriving Regional Fossil Fuel CO_2 Estimates from Atmospheric Observations in a Hot Spot of Nuclear Power Plant $14CO_2$ Emissions, 55, 1555–1576, https://doi.org/10.2458/azu_js_rc.55.16347, 2013.

Wacker, L., Christl, M., and Synal, H. A.: Bats: A new tool for AMS data reduction, Nucl. Instrum. Meth. B, 268, 976–979, https://doi.org/10.1016/j.nimb.2009.10.078, 2010.

Yim, M. S. and Caron, F.: Life cycle and management of carbon-14 from nuclear power generation, Prog. Nucl. Energ., 48, 2–36, https://doi.org/10.1016/j.pnucene.2005.04.002, 2006.

Zellweger, C., Hüglin, C., Klausen, J., Steinbacher, M., Vollmer, M., and Buchmann, B.: Inter-comparison of four different carbon monoxide measurement techniques and evaluation of the long-term carbon monoxide time series of Jungfraujoch, Atmos. Chem. Phys., 9, 3491–3503, https://doi.org/10.5194/acp-9-3491-2009, 2009.

Zellweger, C., Steinbacher, M., and Buchmann, B.: Evaluation of new laser spectrometer techniques for in-situ carbon monoxide measurements, Atmos. Meas. Tech., 5, 2555–2567, https://doi.org/10.5194/amt-5-2555-2012, 2012.

Zondervan, A. and Meijer, H. A. J.: Isotopic characterisation of CO_2 sources during regional pollution events using isotopic and radiocarbon analysis, Tellus B, 48, 601–612, https://doi.org/10.1034/j.1600-0889.1996.00013.x, 1996.